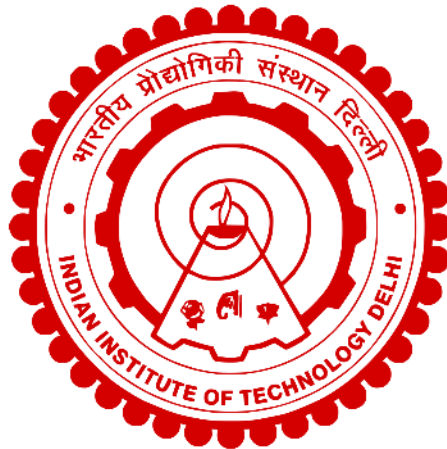


DESIGN, DEVELOPMENT AND CONTROL OF BRUSHLESS DIRECT CURRENT MOTOR DRIVES FOR CEILING FAN

AMIT KUMAR



**DEPARTMENT OF ELECTRICAL ENGINEERING
INDIAN INSTITUTE OF TECHNOLOGY DELHI
HAUZ KHAS, NEW DELHI-110016, INDIA**

July 2025

© Indian Institute of Technology Delhi (IITD), New Delhi, 2025

**DESIGN, DEVELOPMENT AND CONTROL OF
BRUSHLESS DIRECT CURRENT MOTOR DRIVES FOR
CEILING FAN**

by

AMIT KUMAR

Department of Electrical Engineering

Submitted

in fulfillment of the requirements of the degree of
Doctor of Philosophy

to the



**INDIAN INSTITUTE OF TECHNOLOGY DELHI
HAUZ KHAS, NEW DELHI-110016, INDIA**

July 2025

CERTIFICATE

This is to certify that the thesis entitled “**Design, Development and Control of Brushless Direct Current Motor Drives for Ceiling Fan**” being submitted by **Mr. Amit Kumar** for an award of the degree of **Doctor of Philosophy** in the Department of Electrical Engineering, Indian Institute of Technology Delhi, is a record of the research work carried out by him under my supervision and guidance. The matter embodied in this thesis has not been submitted for any other degree or diploma award.

Dated: July 07, 2025

Place: New Delhi

(Prof. Bhim Singh)

**Department of Electrical Engineering
Indian Institute of Technology Delhi,
Hauz Khas, New Delhi-110016, India**

ACKNOWLEDGEMENTS

I wish to express my deepest gratitude and indebtedness to **Prof. Bhim Singh** for providing me guidance and consistent supervision to carry out the Ph.D. work. Working under him has been a wonderful experience, and it has provided me with deep insight into the world of research. Determination, dedication, innovativeness, resourcefulness, and discipline of **Prof. Bhim Singh** have been the inspiration for me to complete this work. His consistent encouragement, continuous monitoring and commitment to excellence have always motivated me to improve my work and use the best of my capabilities. Due to his blessing, I have earned various experiences other than research, which will help me throughout my life.

My sincere thanks and deep gratitude to all S.R.C. members, **Prof. N. Senroy**, and **Prof. Anandarup Das**, Department of Electrical Engineering, and **Prof. Ashu Verma**, Department of Energy Science and Engineering, IIT Delhi, for their valuable guidance and consistent support during my research work. I wish to convey my sincere thanks to **Prof. G. Bhuvaneswari (Mahindra and Mahindra University, Hyderabad)** and **Prof. Ramkrishna Maheswari (University of Southern Denmark, SDU Denmark)**, for providing valuable guidance and necessary support during this work, which made the foundation for my research work.

I wish to express my sincere thanks to the government of India for helping financially under the SERB NSC fellowship. Thanks are due to Mr. Gurcharan Singh, Mr. Srichand, Mr. Puran Singh, Mr. Jitendra, Mr. Boorla Sagar Kumar, Mr. Abhinav Gohar, Mr. Sumit Kumar Singh, Mr. Md. Ale Imran, and Mrs. Neeru Asija of PG Machine Lab, UG & PG Power Electronics Lab, and Communication Lab, IIT Delhi for providing me facilities and assistance during this work. I would also like to thank Mr. Yatindra Mani Tripathi, Mr. Satish Sah, Mr. Sandeep Arora and all other Electrical Engineering office and Lab staff for being supportive throughout the process.

I would like to give special thanks to my batch mates, Mr. Pushpendra Yadav, Dr. Jitendra Gupta, Dr. Souvik Das, and Mr. Utsav Sharma, for their valuable time, motivation, cooperation, and support during my research work. I am also thankful to my seniors, Dr. Utkarsh Sharma, Dr. Shailendra Kumar, Dr. Anshul Varshney, Dr. Radha Kushwaha, Dr. Anjeet Verma, Dr. Vashist Bist, Mr. Saurabh Manglik, and Dr. Rahul Pandey for their valuable aid and cooperation and informal support during this period.

Moreover, I would like to thank my juniors and colleagues, Mr. Saran Kumar Chaurasiya, Mr. Sayandev Ghosh, Mr. Vipin Kumar Singh, Mr. Himansu Sahoo, Mr. Gaurav Kumar, Mr. Rahul Kumar Garg, Mr. Gaurav Kaushik, Mr. Shreyansh Upadhyaya, Mr. Bathala Venugopal, Mr. Abhshek Giri, Mr. Satish Kumar Paturi, Mr. Dattu Suresh and Mr. Nishant Kumar Singh and all PG Machines and PG Power Electronics Lab group for their valuable support. I am thankful to those who have directly or indirectly helped me finish my dissertation study.

Blessings of my father, Late Sh. Hori Lal have always strengthened me in my entire life. My richest love, appreciation and indebtedness go to my mother, Smt. Ganga Devi for her dreams and sacrifices, and wholeheartedly endorses them. Her trust and trust in my capabilities have always motivated me to reach higher academic degrees. I sincerely thank my wife, Mrs. Vineeta, and her elder sister, Mrs. Geeta Kumari, for their continuous support, motivation, and encouragement. Their trust in my capabilities was a key factor in my achievements. I must express my appreciation to my brother, Mr. Khyali Ram, for handling family responsibilities and for his kind support.

At last, I am beholden to the almighty for their blessings to help me to raise my academic level to this stage. I pray for their benediction in my future endeavors. Their blessings may be showered on me for strength, wisdom, and determination to achieve in the future.

Dated: July 07, 2025

Place: New Delhi

Amit Kumar

ABSTRACT

The development of permanent magnet brushless direct current motor (PMBLDCM) drives has focused on energy efficiency and cost reduction, owing to their superior features compared to traditional motors. PMBLDCMs offer high efficiency, high torque to weight ratio, compact size, high power density, silent operation, exceptional reliability, and minimal wear and tear, making them an ideal choice for various low to medium-power applications. These characteristics have led to their widespread use in various household appliances like ceiling fans, mixer juicers, table fans, exhaust fans, and air conditioning.

This thesis aims to develop high-frequency power factor correction (PFC) converters for cost-effective PMBLDCM drives specifically designed for low-power ceiling fan applications. The PMBLDCM relies on a three-phase voltage source inverter (VSI) for electronic commutation, which is facilitated by rotor position sensing using Hall-Effect sensors. Traditional PMBLDCM ceiling fan drive (CFD) operates on a single-phase AC supply through an uncontrolled diode bridge rectifier (DBR), passive PFC, continuous conduction mode (CCM) buck PFC, or CCM flyback PFC, combined with a high value electromagnetic interference filter and DC-link capacitor. This system draws a distorted and peaky current rich in harmonics, resulting in high total harmonic distortion (THD) and an elevated crest-factor in the supply current, leading to a poor power factor (PF) at the supply input. These high current harmonic distortions exceed the limits specified by IEC 61000-3-2 for Class D equipment. To address these issues, single-phase high-frequency AC-DC PFC converters are employed to enhance the power factor and minimize THD at the supply input.

The selection of an appropriate PFC converter for low-power PMBLDCM based CFD depends on various factors, such as the number of components in the converter, the voltage and power ratings of the motor, the need for galvanic isolation, and the overall CFD system cost and efficiency. Based on this, PFC converter configurations are categorized into five types: non-isolated high-frequency PFC converters, isolated high-frequency PFC converters, non-isolated high-frequency integrated PFC converters, isolated high-frequency integrated PFC converters, and high-frequency bridgeless non-isolated/isolated PFC converters. High-frequency bridgeless configurations are specifically designed to reduce conduction losses in the front-end high-frequency PFC converter by partially or fully eliminating the diode bridge rectifier. Additionally,

the control strategy of the high-frequency PFC converter plays a crucial role in determining the overall CFD system's performance and cost. In this work, high-frequency PFC converters are designed to achieve high step-down gain with their desired operating duties and operate in discontinuous inductor current mode (DICM). The DC-link voltage of these high-frequency PFC converters is controlled using a voltage follower approach, eliminating the need for voltage and current sensors.

This work presents the analysis, design, DICM modeling, and control of buck-boost categorized high-frequency PFC converters to enhance power quality at the supply input of a PMBLDCM based CFD. A key focus is placed on simplifying control mechanisms, minimizing the number of sensors, reducing costs, and improving the overall efficiency of the CFD system. Additionally, some new configurations of single-phase high-frequency AC-DC PFC converters are proposed for powering the PMBLDCM drive used in ceiling fan applications. The speed of the PMBLDCM is controlled by adjusting the DC-link voltage of the VSI, which drives the PMBLDCM. This approach enables the VSI to operate with fundamental frequency switching, thereby reducing switching losses.

A novel sensorless control method for high-frequency AC-DC PFC converters is also developed to control the DC-link voltage. Additionally, a simple back-EMF-based sensorless control approach for the PMBLDCM is designed, allowing variable DC-link voltage control for speed change of the motor. The performance of these high-frequency PFC converters fed PMBLDCM based CFDs is validated through models created in the MATLAB/Simulink environment. Experimental verification is also conducted using a laboratory-developed hardware prototype of the sensorless high-frequency PFC converters feeding PMBLDCM based CFD. Performance evaluation encompasses steady-state performance at different operating speeds, dynamic performance during speed change, and robustness against supply voltage fluctuations at the AC supply input. Steady-state analysis includes the voltage and current key waveforms of high-frequency PFC converter components (MOSFET switch, inductor, high-frequency transformer, diode, and capacitor) to establish component selection criteria. Furthermore, the presented high-frequency PFC converters demonstrate compliance with power quality standards, maintaining supply current harmonic distortion within limits specified by IEC 61000-3-2 for Class D. These findings underscore the potential of the presented high-frequency PFC based PMBLDCM drives as energy-efficient, cost-effective, and high-performance solutions for ceiling fan applications.

सार

स्थायी चुंबक ब्रशलेस डायरेक्ट करंट मोटर (पीएमबीएलडीसीएम) ड्राइव के विकास ने ऊर्जा दक्षता और लागत में कमी पर ध्यान केंद्रित किया है, क्योंकि पारंपरिक मोटरों की तुलना में ये बेहतर विशेषताएं प्रदान करते हैं। पीएमबीएलडीसीएम उच्च दक्षता, उच्च बलाघूर्ण-भार अनुपात, जटिल आकार, उच्च शक्ति घनत्व, शांत संचालन, असाधारण विश्वसनीयता और न्यूनतम टूट-फूट प्रदान करते हैं, जो उन्हें विभिन्न निम्न से मध्यम-शक्ति अनुप्रयोगों के लिए एक आदर्श विकल्प बनाता है। इन विशेषताओं के कारण इनका उपयोग विभिन्न घरेलू उपकरणों जैसे छत का पंखा, रस निकालने का उपकरण, मेज़ का पंखा, निष्कासक पंखा और वातानुकूलन में व्यापक रूप से किया जाता है।

इस शोध प्रबंध का उद्देश्य विशेष रूप से कम-शक्ति वाले छत के पंखों के अनुप्रयोगों के लिए डिज़ाइन किए गए लागत-प्रभावी पीएमबीएलडीसीएम ड्राइव के लिए उच्च-आवृत्ति पावर फैक्टर करेक्शन (पीएफसी) कनवर्टर विकसित करना है। पीएमबीएलडीसीएम इलेक्ट्रॉनिक कम्यूटेशन के लिए तीन-चरण वोल्टेज स्रोत इन्वर्टर (वीएसआई) पर निर्भर करता है, जिसे हॉल-इफेक्ट सेंसर का उपयोग करके रोटार स्थिति संवेदन द्वारा सुगम बनाया जाता है। पारंपरिक पीएमबीएलडीसीएम सीलिंग फैन ड्राइव (सीएफडी) एक अनियंत्रित डायोड ब्रिज रेक्टिफायर (डीबीआर), पैसिव पीएफसी, कंटीन्यूअस कंडक्शन मोड (सीसीएम) बक पीएफसी, या सीसीएम फ्लाइबैक पीएफसी के माध्यम से एकल-फेज एसी आपूर्ति पर संचालित होता है, जिसे उच्च मान वाले इलेक्ट्रोमैग्नेटिक इंटरफेरेंस फ़िल्टर और डीसी-लिंक कैपेसिटर के साथ जोड़ा जाता है। यह प्रणाली हार्मोनिक्स से भरपूर एक विकृत और चरम धारा खींचती है, जिसके परिणामस्वरूप उच्च टोटल हार्मोनिक डिस्टॉर्शन (टीएचडी) और आपूर्ति धारा में एक उच्च क्रेस्ट-फैक्टर होता है, जिससे आपूर्ति इनपुट पर एक खराब पावर फैक्टर (पीएफ) होता है। ये उच्च धारा हार्मोनिक विकृतियाँ आईईसी. ६१०००-३-२ द्वारा वर्ग डी उपकरणों के लिए निर्दिष्ट सीमाओं से अधिक हैं। इन समस्याओं के समाधान के लिए, आपूर्ति इनपुट पर पावर फैक्टर को बढ़ाने और टीएचडी को न्यूनतम करने के लिए एकल-फेज उच्च-आवृत्ति एसी-डीसी पीएफसी कन्वर्टर्स का उपयोग किया जाता है।

कम-शक्ति वाले पीएमबीएलडीसीएम आधारित सीएफडी के लिए उपयुक्त पीएफसी कनवर्टर का चयन कई कारकों पर निर्भर करता है, जैसे कनवर्टर में घटकों की संख्या, मोटर की वोल्टेज और पावर रेटिंग, गैल्वेनिक आइसोलेशन की आवश्यकता, और समग्र सीएफडी प्रणाली की लागत और दक्षता। इसके आधार पर, पीएफसी कनवर्टर विन्यास को पाँच प्रकारों में वर्गीकृत किया गया है: गैर-पृथक उच्च-आवृत्ति पीएफसी कनवर्टर, पृथक उच्च-आवृत्ति पीएफसी कनवर्टर, गैर-पृथक उच्च-आवृत्ति एकीकृत पीएफसी कनवर्टर, पृथक उच्च-आवृत्ति एकीकृत पीएफसी कनवर्टर, और उच्च-आवृत्ति ब्रिजलेस गैर-पृथक/पृथक पीएफसी कनवर्टर। उच्च-आवृत्ति ब्रिजलेस विन्यास विशेष रूप से डायोड ब्रिज रेक्टिफायर को आंशिक या पूर्ण रूप से हटाकर फ्रंट-एंड उच्च-आवृत्ति पीएफसी कनवर्टर में चालन हानि को कम करने के लिए डिज़ाइन किए गए हैं। इसके अतिरिक्त, उच्च-आवृत्ति पीएफसी कनवर्टर की नियंत्रण रणनीति समग्र सीएफडी प्रणाली के प्रदर्शन और लागत को निर्धारित करने में महत्वपूर्ण भूमिका निभाती है। इस कार्य में, उच्च-आवृत्ति वाले पीएफसी कन्वर्टर्स को उनके वांछित परिचालन कर्तव्यों के साथ उच्च

स्टेप-डाउन लाभ प्राप्त करने और असंतत प्रेरक धारा मोड (डीआईसीएम) में संचालित करने के लिए डिजाइन किया गया है। इन उच्च-आवृत्ति वाले पीएफसी कन्वर्टर के डीसी-लिंक वोल्टेज को वोल्टेज फॉलोअर दृष्टिकोण का उपयोग करके नियंत्रित किया जाता है, जिससे वोल्टेज और धारा सेंसर की आवश्यकता समाप्त हो जाती है।

यह कार्य पीएमबीएलडीसीएम आधारित सीएफडी के आपूर्ति इनपुट पर विद्युत गुणवत्ता बढ़ाने के लिए बक-बूस्ट श्रेणीबद्ध उच्च-आवृत्ति वाले पीएफसी कन्वर्टर का विश्लेषण, डिजाइन, डीआईसीएम मॉडलिंग और नियंत्रण प्रस्तुत करता है। नियंत्रण तंत्र को सरल बनाने, सेंसरों की संख्या को कम करने, लागत कम करने और सीएफडी प्रणाली की समग्र दक्षता में सुधार करने पर मुख्य ध्यान केंद्रित किया गया है। इसके अतिरिक्त, सीलिंग फैन अनुप्रयोगों में उपयोग किए जाने वाले पीएमबीएलडीसीएम ड्राइव को शक्ति प्रदान करने के लिए एकल-चरण उच्च-आवृत्ति वाले एसी-डीसी पीएफसी कन्वर्टर के कुछ नए विन्यास प्रस्तावित किए गए हैं। पीएमबीएलडीसीएम की गति को वीएसआई के डीसी-लिंक वोल्टेज को समायोजित करके नियंत्रित किया जाता है, जो पीएमबीएलडीसीएम को चलाता है। यह दृष्टिकोण वीएसआई को मूल आवृत्ति स्विचिंग के साथ संचालित करने में सक्षम बनाता है, जिससे स्विचिंग हानियाँ कम होती हैं।

उच्च-आवृत्ति वाले एसी-डीसी पीएफसी कन्वर्टर के लिए डीसी-लिंक वोल्टेज को नियंत्रित करने हेतु एक नवीन सेंसर रहित नियंत्रण विधि भी विकसित की गई है। इसके अतिरिक्त, पीएमबीएलडीसीएम के लिए एक सरल बैक-ईएमएफ-आधारित सेंसर रहित नियंत्रण दृष्टिकोण डिजाइन किया गया है, जो मोटर की गति परिवर्तन के लिए परिवर्तनशील डीसी-लिंक वोल्टेज नियंत्रण की अनुमति देता है। पीएमबीएलडीसीएम आधारित सीएफडी से पोषित इन उच्च-आवृत्ति वाले पीएफसी कन्वर्टर के प्रदर्शन का सत्यापन मैटलैब/सिमुलिक वातावरण में निर्मित मॉडलों के माध्यम से किया जाता है। पीएमबीएलडीसीएम आधारित सीएफडी से पोषित सेंसर रहित उच्च-आवृत्ति वाले पीएफसी कन्वर्टर के प्रयोगशाला-विकसित हार्डवेयर प्रोटोटाइप का उपयोग करके प्रायोगिक सत्यापन भी किया जाता है। प्रदर्शन मूल्यांकन में विभिन्न परिचालन गतियों पर स्थिर-अवस्था प्रदर्शन, गति परिवर्तन के दौरान गतिशील प्रदर्शन, और एसी आपूर्ति इनपुट पर आपूर्ति वोल्टेज में उतार-चढ़ाव के प्रति मजबूती शामिल है। स्थिर-अवस्था विश्लेषण में घटक चयन मानदंड स्थापित करने के लिए उच्च आवृत्ति पीएफसी कन्वर्टर घटकों (एमओएसएफईटी स्विच, प्रारंभ करनेवाला, उच्च आवृत्ति ट्रांसफार्मर, डायोड और संधारित्र) के वोल्टेज और वर्तमान प्रमुख तरंगों को शामिल किया जाता है। इसके अलावा, प्रस्तुत उच्च-आवृत्ति पीएफसी कन्वर्टर विद्युत गुणवत्ता मानकों के अनुपालन को प्रदर्शित करते हैं, तथा आपूर्ति धारा हार्मोनिक विरूपण को वर्ग डी के लिए आईईसी. ६१०००-३-२ द्वारा निर्दिष्ट सीमाओं के भीतर बनाए रखते हैं। ये निष्कर्ष छत पंखा अनुप्रयोगों के लिए ऊर्जा-कुशल, लागत-प्रभावी और उच्च-प्रदर्शन समाधान के रूप में प्रस्तुत उच्च-आवृत्ति पीएफसी आधारित पीएमबीएलडीसीएम ड्राइव की क्षमता को रेखांकित करते हैं।

TABLE OF CONTENTS

| | | |
|-----------------------|---|-------------|
| Certificate | i | |
| Acknowledgements | iii | |
| Abstract | v | |
| Table of Contents | ix | |
| List of Figures | xxv | |
| List of Tables | xxxix | |
| List of Abbreviations | xliii | |
| List of Symbols | xlvi | |
| | | |
| CHAPTER-I | INTRODUCTION | 1-14 |
| 1.1 | General | 1 |
| 1.2 | State of Art on Permanent Magnet Brushless Direct Current Motor Based Ceiling Fan Drive | 1 |
| 1.2.1 | Development of PMBLDCM Based Ceiling Fan Drive | 2 |
| 1.2.2 | Control of PMBLDCM Based Ceiling Fan Drive | 3 |
| 1.2.3 | Potential Applications of PMBLDC Motors | 5 |
| 1.3 | Power Quality Issues in Permanent Magnet Brushless Direct Current Motor Based Ceiling Fan Drive | 5 |
| 1.3.1 | Power Quality Issues in a DBR fed PMBLDCM Based Ceiling Fan Drive | 6 |
| 1.3.2 | Power Quality Issues in the Passive-PFC fed PMBLDCM Based Ceiling Fan Drive | 6 |
| 1.3.3 | Power Quality Issues in the Buck-PFC fed PMBLDCM Based Ceiling Fan Drive | 6 |
| 1.3.4 | Power Quality Issues in the Flyback-PFC fed PMBLDCM Based Ceiling Fan Drive | 8 |

| | | |
|---|--|--------------|
| 1.3.5 | Power Quality Standard | 8 |
| 1.3.6 | Power Quality Improvement in PFC Converters Fed PMBLDCM Based Ceiling Fan Drive | 9 |
| 1.4 | Objectives and Scope of Work | 10 |
| 1.4.1 | Comparative Analysis of Various Low Power Drives for Ceiling Fan | 10 |
| 1.4.2 | Analysis, Design, Modeling and Development of PFC Converters Fed PMBLDCM Based Ceiling Fan Drives | 10 |
| 1.4.3 | Analysis, Design, Modeling and Development of Sensorless PFC Converters Fed PMBLDCM Based Ceiling Fan Drives | 10 |
| 1.5 | Outline of Chapters | 12 |
| CHAPTER-II LITERATURE REVIEW | | 15-28 |
| 2.1 | General | 15 |
| 2.2 | Literature Survey | 16 |
| 2.2.1 | Review of Low Power Drives for Ceiling Fan | 16 |
| 2.2.2 | Review of Low Power PMBLDCM Drives | 17 |
| 2.2.3 | Review of Sensorless Control of Low Power PMBLDCM Drives | 19 |
| 2.2.4 | Review of PFC Converters for Low Power PMBLDCM Drive | 20 |
| 2.2.5 | Review of PFC Converters Fed PMBLDCM Drives for Ceiling Fan | 25 |
| 2.3 | Identified Research Area | 26 |
| 2.4 | Conclusions | 28 |
| CHAPTER-III COMPARATIVE ANALYSIS OF VARIOUS LOW-POWER DRIVES FOR CEILING FAN | | 29-48 |
| 3.1 | General | 29 |
| 3.2 | Needs of Low Power Drives for Ceiling Fan | 29 |
| 3.2.1 | Low Power Drives Used in Ceiling Fan | 29 |

| | | |
|---------|--|----|
| 3.2.1.1 | Permanent-Split Capacitor Induction Motor Based CFD and its Control | 30 |
| 3.2.1.2 | Switched Reluctance Motor Based CFD and its Control | 31 |
| 3.2.1.3 | Permanent Magnet Synchronous Motor Based CFD and its Control | 32 |
| 3.2.1.4 | PMBLDC Motor Based CFD and its Control | 34 |
| 3.3 | Comparative Features of Low Power Drives for Ceiling Fans | 35 |
| 3.3.1 | Comparison Based on Fixed and Operating Costs | 36 |
| 3.3.2 | Comparison Based on Control Complexity | 37 |
| 3.3.3 | Comparison Based on Drives Lifespan and Maintenance | 37 |
| 3.3.4 | Comparison Based on Speed Control and Noise | 38 |
| 3.4 | MATLAB Simulation Study of Low Power Drives for Ceiling Fan | 39 |
| 3.4.1 | Simulation Study of Permanent-Split Capacitor Induction Motor Based CFD | 39 |
| 3.4.2 | Simulation Study of Switched Reluctance Motor Based CFD | 40 |
| 3.4.3 | Simulation Study of Permanent Magnet Synchronous Motor Based CFD | 41 |
| 3.4.4 | Simulation Study of PMBLDCM Based CFD | 42 |
| 3.5 | Experimental Performance of Market Available Low Power CFDs | 43 |
| 3.5.1 | Experimental Test Performance of Permanent-Split Capacitor Induction Motor Based CFD | 43 |
| 3.5.2 | Experimental Test Performance of PMBLDCM Based CFD | 45 |
| 3.6 | Conclusions | 47 |

CHAPTER-IV DESIGN, CONTROL AND IMPLEMENTATION OF 49-92
HIGH-FREQUENCY NON-ISOLATED AC-DC PFC
CONVERTERS FED SENSORLESS PMBLDCM
BASED CEILING FAN DRIVES

| | | |
|---------|--|----|
| 4.1 | General | 49 |
| 4.2 | Configurations, Operation, and Analysis of Non-Isolated AC-DC PFC Converters Fed PMBLDCM Based CFDs | 49 |
| 4.2.1 | Non-Isolated Switched Inductor AC-DC Zeta PFC Converter Fed Sensorless PMBLDCM Based CFD | 49 |
| 4.2.1.1 | DICM Operating Conditions of SI-Zeta PFC Converter | 53 |
| 4.2.1.2 | Small-Signal Modeling of SI-Zeta PFC Converter | 53 |
| 4.2.2 | Non-Isolated Switched Inductor AC-DC Cuk PFC Converter Fed Sensorless PMBLDCM Based CFD | 56 |
| 4.2.2.1 | DICM Operating Conditions of SIC PFC Converter | 60 |
| 4.2.2.2 | Small-Signal Modeling of SIC PFC Converter | 60 |
| 4.3 | Design of Non-Isolated AC-DC PFC Converters Fed PMBLDCM Based CFDs | 63 |
| 4.3.1 | Non-Isolated Switched Inductor AC-DC Zeta PFC Converter Fed Sensorless PMBLDCM Based CFD | 65 |
| 4.3.2 | Non-Isolated Switched Inductor AC-DC Cuk PFC Converter Fed Sensorless PMBLDCM Based CFD | 67 |
| 4.3.2.1 | Coupled Inductor Design for Sensorless Switched Inductor AC-DC Cuk PFC Converter Fed PMBLDCM Based CFD | 69 |
| 4.4 | Control of Non-Isolated AC-DC PFC Converters Fed PMBLDCM Based CFDs | 71 |
| 4.4.1 | Non-Isolated Switched Inductor AC-DC Zeta PFC Converter Fed Sensorless PMBLDCM Based CFD | 71 |
| 4.4.1.1 | Converter Voltage Control and its Design Using MATLAB | 72 |
| 4.4.1.2 | Sensorless Control of PMBLDCM | 73 |
| 4.4.2 | Coupled Inductor Based Sensorless Non-Isolated Switched Inductor AC-DC Cuk PFC Converter Fed PMBLDCM Based CFD | 74 |
| 4.4.2.1 | Converter Voltage Control and its Design Using MATLAB | 74 |

| | | |
|---------|---|----|
| 4.4.2.2 | Sensorless Control of PMBLDCM | 76 |
| 4.5 | MATLAB Based Modeling and Simulation of Non-Isolated AC-DC PFC Converters Fed Sensorless PMBLDCM Based CFDs | 77 |
| 4.5.1 | Non-Isolated Switched Inductor AC-DC Zeta PFC Converter Fed Sensorless PMBLDCM Based CFD | 77 |
| 4.5.2 | Coupled Inductor Based Sensorless Non-Isolated Switched Inductor AC-DC Cuk PFC Converter Fed PMBLDCM Based CFD | 78 |
| 4.6 | Hardware Implementation of Non-Isolated AC-DC PFC Converters Fed Sensorless PMBLDCM Based CFDs | 78 |
| 4.6.1 | Hardware Implementation of Non-Isolated Switched Inductor AC-DC Zeta PFC Converter Fed Sensorless PMBLDCM Based CFD | 79 |
| 4.6.2 | Hardware Implementation of Sensorless Coupled Inductor Based Non-Isolated Switched Inductor AC-DC Cuk PFC Converter Fed PMBLDCM Based CFD | 80 |
| 4.7 | Results and Discussion | 81 |
| 4.7.1 | Performance of Non-Isolated Switched Inductor AC-DC Zeta PFC Converter Fed Sensorless PMBLDCM Based CFD | 81 |
| 4.7.1.1 | Steady State Performance | 81 |
| 4.7.1.2 | Dynamic Performance With Supply Voltage Fluctuations | 83 |
| 4.7.1.3 | Dynamic Performance With Speed Control | 83 |
| 4.7.1.4 | Performance Comparisons at Different Operating Speeds | 84 |
| 4.7.2 | Performance of Sensorless Coupled Inductor Based Non-Isolated Switched Inductor AC-DC Cuk PFC Converter Fed PMBLDCM Based CFD | 86 |
| 4.7.2.1 | Steady State Performance | 86 |
| 4.7.2.2 | Dynamic Performance With Supply Voltage Fluctuations | 87 |
| 4.7.2.3 | Dynamic Performance With Speed Control | 88 |
| 4.7.2.4 | Performance Comparisons at Different Operating Speeds | 89 |

| | | |
|------------------|---|---------------|
| 4.8 | Comparative Evaluation of Non-Isolated Switched Inductor AC-DC PFC Converters Fed Sensorless PMBLDCM Based CFDs | 90 |
| 4.9 | Conclusions | 91 |
| CHAPTER-V | DESIGN, CONTROL AND IMPLEMENTATION OF HIGH-FREQUENCY SENSORLESS ISOLATED AC-DC PFC CONVERTERS FED PMBLDCM BASED CEILING FAN DRIVES | 93-133 |
| 5.1 | General | 93 |
| 5.2 | Configurations, Operation, and Analysis of Sensorless Isolated AC-DC PFC Converters Fed PMBLDCM Based CFDs | 93 |
| 5.2.1 | Sensorless Isolated AC-DC Zeta PFC Converter Fed PMBLDCM Based CFD | 94 |
| 5.2.2 | Sensorless Isolated AC-DC SEPIC PFC Converter Fed PMBLDCM Based CFD | 97 |
| 5.2.3 | Sensorless Isolated AC-DC Cuk PFC Converter Fed PMBLDCM Based CFD | 101 |
| 5.3 | Design of Sensorless Isolated AC-DC PFC Converters Fed PMBLDCM Based CFDs | 103 |
| 5.3.1 | Design of Sensorless Isolated AC-DC Zeta PFC Converter Fed PMBLDCM Based CFD | 104 |
| 5.3.2 | Design of Sensorless Isolated AC-DC SEPIC PFC Converter Fed PMBLDCM Based CFD | 106 |
| 5.3.3 | Design of Sensorless Isolated AC-DC Cuk PFC Converter Fed PMBLDCM Based CFD | 108 |
| 5.4 | Control of Sensorless Isolated AC-DC PFC Converters Fed PMBLDCM Based CFDs | 110 |
| 5.4.1 | Voltage Control of Isolated AC-DC PFC Converters | 110 |

| | | |
|---------|---|-----|
| 5.4.2 | Back-EMF Based Sensorless Control of PMBLDCM | 111 |
| 5.5 | MATLAB Based Modeling and Simulation of Sensorless Isolated AC-DC PFC Converters Fed PMBLDCM Based CFDs | 112 |
| 5.5.1 | MATLAB Based Model of Sensorless Isolated AC-DC Zeta PFC Converter | 113 |
| 5.5.2 | MATLAB Based Model of Sensorless Isolated AC-DC SEPIC PFC Converter | 113 |
| 5.5.3 | MATLAB Based Model of Sensorless Isolated AC-DC Cuk PFC Converter | 114 |
| 5.6 | Hardware Implementation of Sensorless Isolated AC-DC PFC Converters Fed PMBLDCM Based CFDs | 114 |
| 5.6.1 | Hardware Implementation of Sensorless Isolated AC-DC Zeta PFC Converter Fed PMBLDCM Based CFD | 115 |
| 5.6.2 | Hardware Implementation of Sensorless Isolated AC-DC SEPIC PFC Converter Fed PMBLDCM Based CFD | 116 |
| 5.6.3 | Hardware Implementation of Sensorless Isolated AC-DC Cuk PFC Converter Fed PMBLDCM Based CFD | 118 |
| 5.7 | Results and Discussion | 119 |
| 5.7.1 | Performance of Sensorless Isolated AC-DC Zeta PFC Converter Fed PMBLDCM Based CFD | 120 |
| 5.7.1.1 | Steady State Performance | 120 |
| 5.7.1.2 | Dynamic Performance With Supply Voltage Fluctuations | 122 |
| 5.7.1.3 | Dynamic Performance With Speed Control | 122 |
| 5.7.1.4 | Performance Comparisons at Different Operating Speeds | 123 |
| 5.7.2 | Performance of Sensorless Isolated AC-DC SEPIC PFC Converter Fed PMBLDCM Based CFD | 125 |
| 5.7.2.1 | Steady State Performance | 125 |
| 5.7.2.2 | Dynamic Performance With Supply Voltage Fluctuations | 126 |

| | | |
|-------------------|---|----------------|
| 5.7.2.3 | Dynamic Performance With Speed Control | 127 |
| 5.7.3 | Performance of Sensorless Isolated AC-DC Cuk PFC Converter Fed PMBLDCM Based CFD | 128 |
| 5.7.3.1 | Steady State Performance | 128 |
| 5.7.3.2 | Dynamic Performance With Supply Voltage Fluctuations | 130 |
| 5.7.3.3 | Dynamic Performance With Speed Control | 130 |
| 5.8 | Comparative Evaluation of Sensorless Isolated AC-DC PFC Converters Fed PMBLDCM Based CFDs | 132 |
| 5.9 | Conclusions | 132 |
| CHAPTER-VI | DESIGN, CONTROL AND IMPLEMENTATION OF HIGH-FREQUENCY SENSORLESS INTEGRATED SINGLE-STAGE SINGLE-SWITCH NON-ISOLATED AC-DC PFC CONVERTERS FED PMBLDCM BASED CEILING FAN DRIVES | 135-182 |
| 6.1 | General | 135 |
| 6.2 | Configurations, Operation, and Analysis of Sensorless Integrated Single-Switch Non-Isolated AC-DC PFC Converters Fed PMBLDCM Based CFDs | 135 |
| 6.2.1 | Sensorless Integrated Single-Switch Non-Isolated SI-Buck-Flyback AC-DC PFC Converter Fed PMBLDCM BASED CFD | 135 |
| 6.2.1.1 | Small-Signal Modeling of Single-Switch SI-Buck-Flyback PFC Converter | 142 |
| 6.2.2 | Sensorless Integrated Non-Isolated Single-Switch SEPIC-SC AC-DC PFC Converter Fed PMBLDCM BASED CFD | 146 |
| 6.2.2.1 | DICM Operating Conditions of Single-Switch SEPIC-SC PFC Converter | 151 |
| 6.2.2.2 | Small-Signal Modeling of Single-Switch SEPIC-SC PFC Converter | 152 |

| | | |
|---------|---|-----|
| 6.3 | Design of Integrated Single-Switch Non-Isolated AC-DC PFC Converters Fed PMBLDCM Based CFDs | 153 |
| 6.3.1 | Sensorless Integrated Non-Isolated Single-Switch SI-Buck-Flyback AC-DC PFC Converter Fed PMBLDCM Based CFD | 155 |
| 6.3.2 | Sensorless Integrated Non-Isolated Single-Switch SEPIC-SC AC-DC PFC Converter Fed PMBLDCM Based CFD | 156 |
| 6.4 | Control of Sensorless Integrated Single-Switch Non-Isolated AC-DC PFC Converters Fed PMBLDCM Based CFDs | 158 |
| 6.4.1 | Sensorless Integrated Non-Isolated Single-Switch SI-Buck-Flyback AC-DC PFC Converter Fed PMBLDCM Based CFD | 159 |
| 6.4.1.1 | Converter Voltage Control and its Design Using MATLAB | 159 |
| 6.4.1.2 | Sensorless Control of PMBLDCM | 160 |
| 6.4.2 | Sensorless Integrated Non-Isolated Single-Switch SEPIC-SC AC-DC PFC Converter Fed PMBLDCM Based CFD | 161 |
| 6.4.2.1 | Converter Voltage Control and its Design Using MATLAB | 162 |
| 6.4.2.2 | Sensorless Control of PMBLDCM | 163 |
| 6.5 | MATLAB Based Modeling and Simulation of Integrated Single-Switch Non-Isolated AC-DC PFC Converters Fed PMBLDCM Based CFDs | 164 |
| 6.5.1 | Sensorless Integrated Non-Isolated Single-Switch SI-Buck-Flyback AC-DC PFC Converter Fed PMBLDCM Based CFD | 164 |
| 6.5.2 | Sensorless Integrated Non-Isolated Single-Switch SEPIC-SC AC-DC PFC Converter Fed PMBLDCM Based CFD | 164 |
| 6.6 | Hardware Implementation of Sensorless Integrated Single-Switch Non-Isolated AC-DC PFC Converters Fed PMBLDCM Based CFDs | 165 |
| 6.6.1 | Sensorless Integrated Non-Isolated Single-Switch SI-Buck-Flyback PFC Converter Fed PMBLDCM Based CFD | 165 |
| 6.6.2 | Sensorless Integrated Non-Isolated Single-Switch SEPIC-SC PFC Converter Fed PMBLDCM Based CFD | 167 |

| | | |
|---------|--|-----|
| 6.7 | Results and Discussion | 168 |
| 6.7.1 | Performance of Sensorless Integrated Non-Isolated Single-Switch SI-Buck-Flyback PFC Converter Fed PMBLDCM Based CFD | 168 |
| 6.7.1.1 | Steady State Performance | 169 |
| 6.7.1.2 | Dynamic Performance With Supply Voltage Fluctuations | 170 |
| 6.7.1.3 | Dynamic Performance With Speed Control | 171 |
| 6.7.1.4 | Performance Comparisons at Different Operating Speeds | 172 |
| 6.7.2 | Performance of Sensorless Integrated Non-Isolated Single-Switch SEPIC-SC PFC Converter Fed PMBLDCM Based CFD | 175 |
| 6.7.2.1 | Steady State Performance | 175 |
| 6.7.2.2 | Dynamic Performance With Supply Voltage Fluctuations | 177 |
| 6.7.2.3 | Dynamic Performance With Speed Control | 177 |
| 6.7.2.4 | Performance Comparisons at Different Operating Speeds | 178 |
| 6.8 | Comparative Evaluation of Sensorless Integrated Non-Isolated Single-Switch AC-DC PFC Converters Fed PMBLDCM Based CFDs | 180 |
| 6.9 | Conclusions | 181 |

CHAPTER-VII DESIGN, CONTROL AND IMPLEMENTATION OF 183-260
HIGH-FREQUENCY SENSORLESS INTEGRATED
SINGLE-STAGE SINGLE-SWITCH ISOLATED AC-
DC PFC CONVERTERS FED PMBLDCM BASED
CEILING FAN DRIVES

| | | |
|-------|--|-----|
| 7.1 | General | 183 |
| 7.2 | Configurations, Operation, and Analysis of Sensorless Integrated Single-Switch Isolated AC-DC PFC Converters Fed PMBLDCM Based CFD | 183 |
| 7.2.1 | Sensorless Integrated Single-Switch Isolated Boost-Flyback AC-DC PFC Converter Fed PMBLDCM Based CFD | 184 |

| | | |
|---------|--|-----|
| 7.2.1.1 | DICM Operating Conditions of Single-Switch Isolated Boost-Flyback PFC Converter | 189 |
| 7.2.1.2 | Small-Signal Modeling of Single-Switch Isolated Boost-Flyback PFC Converter | 190 |
| 7.2.2 | Sensorless Integrated Single-Switch Isolated Boost-Luo AC-DC PFC Converter Fed PMBLDCM Based CFD | 191 |
| 7.2.3 | Sensorless Integrated Single-Switch Isolated SEPIC-Forward AC-DC PFC Converter Fed PMBLDCM Based CFD | 196 |
| 7.2.4 | Sensorless Integrated Single-Switch Isolated Buck-Flyback AC-DC PFC Converter Fed PMBLDCM Based CFD | 202 |
| 7.2.4.1 | DICM Operating Conditions of Single-Switch Isolated Buck-Flyback PFC Converter | 207 |
| 7.2.4.2 | Small-Signal Modeling of Single-Switch Isolated Buck-Flyback PFC Converter | 208 |
| 7.3 | Design of Sensorless Integrated Single-Switch Isolated AC-DC PFC Converters Fed PMBLDCM Based CFDs | 209 |
| 7.3.1 | Sensorless Integrated Single-Switch Isolated Boost-Flyback AC-DC PFC Converter Fed PMBLDCM Based CFD | 210 |
| 7.3.2 | Sensorless Integrated Single-Switch Isolated Boost-Luo AC-DC PFC Converter Fed PMBLDCM Based CFD | 214 |
| 7.3.3 | Sensorless Integrated Single-Switch Isolated SEPIC-Forward AC-DC PFC Converter Fed PMBLDCM Based CFD | 216 |
| 7.3.4 | Sensorless Integrated Single-Switch Isolated Buck-Flyback AC-DC PFC Converter Fed PMBLDCM Based CFD | 218 |
| 7.4 | Control of Sensorless Integrated Single-Switch Isolated AC-DC PFC Converters Fed PMBLDCM Based CFDs | 219 |
| 7.4.1 | Sensorless Voltage Control of an Integrated Single-Switch Isolated AC-DC PFC Converters | 219 |

| | | |
|---------|--|-----|
| 7.4.1.1 | Controller Design of Single-Switch Isolated Boost-Flyback PFC Converter | 221 |
| 7.4.1.2 | Controller Design of Single-Switch Isolated Boost-Luo PFC Converter | 221 |
| 7.4.1.3 | Controller Design of Single-Switch Isolated SEPIC-Forward PFC Converter | 222 |
| 7.4.1.4 | Controller Design of Single-Switch Isolated Buck-Flyback PFC Converter | 222 |
| 7.4.2 | Back-EMF Based Sensorless Control of PMBLDCM | 223 |
| 7.5 | MATLAB Based Modeling and Simulation of Sensorless Integrated Single-Switch Isolated AC-DC PFC Converters Fed PMBLDCM Based CFDs | 224 |
| 7.5.1 | MATLAB Model of Sensorless Integrated Single-Switch Isolated Boost-Flyback PFC Converter | 225 |
| 7.5.2 | MATLAB Model of Sensorless Integrated Single-Switch Isolated Boost-Luo PFC Converter | 226 |
| 7.5.3 | MATLAB Model of Sensorless Integrated Single-Switch Isolated SEPIC-Forward PFC Converter | 226 |
| 7.5.4 | MATLAB Model of Sensorless Integrated Single-Switch Isolated Buck-Flyback PFC Converter | 227 |
| 7.6 | Hardware Implementation of Sensorless Integrated Single-Switch Isolated AC-DC PFC Converters Fed PMBLDCM Based CFDs | 228 |
| 7.6.1 | Hardware Implementation of Sensorless Integrated Single-Switch Isolated Boost-Flyback AC-DC PFC Converter Fed PMBLDCM Based CFD | 228 |
| 7.6.2 | Hardware Implementation of Sensorless Integrated Single-Switch Isolated Boost-Luo AC-DC PFC Converter Fed PMBLDCM Based CFD | 230 |

| | | |
|---------|---|-----|
| 7.6.3 | Hardware Implementation of Sensorless Integrated Single-Switch Isolated SEPIC-Forward AC-DC PFC Converter Fed PMBLDCM Based CFD | 232 |
| 7.6.4 | Hardware Implementation of Sensorless Integrated Single-Switch Isolated Buck-Flyback AC-DC PFC Converter Fed PMBLDCM Based CFD | 233 |
| 7.7 | Results and Discussion | 235 |
| 7.7.1 | Performance of Sensorless Integrated Single-Switch Isolated Boost-Flyback AC-DC PFC Converter Fed PMBLDCM Based CFD | 235 |
| 7.7.1.1 | Steady State Performance | 235 |
| 7.7.1.2 | Dynamic Performance With Supply Voltage Fluctuations | 237 |
| 7.7.1.3 | Dynamic Performance With Speed Control | 237 |
| 7.7.1.4 | Performance Comparisons at Different Operating Speeds | 239 |
| 7.7.2 | Performance of Sensorless Integrated Single-Switch Isolated Boost-Luo AC-DC PFC Converter Fed PMBLDCM Based CFD | 241 |
| 7.7.2.1 | Steady State Performance | 241 |
| 7.7.2.2 | Dynamic Performance With Supply Voltage Fluctuations | 243 |
| 7.7.2.3 | Performance Comparisons at Different Operating Speeds | 244 |
| 7.7.3 | Performance of Sensorless Integrated Single-Switch Isolated SEPIC-Forward AC-DC PFC Converter Fed PMBLDCM Based CFD | 246 |
| 7.7.3.1 | Performance of 48V PMBLDCM Solar CFD | 246 |
| 7.7.3.2 | Steady-State Performance of SEPIC-Forward Based 48V PMBLDCM CFD | 247 |
| 7.7.3.3 | Dynamic Performance of SEPIC-Forward Based 48V PMBLDCM CFD with Speed Control | 249 |
| 7.7.3.4 | Performance Comparisons at Different Operating Speeds | 250 |
| 7.7.4 | Performance of Sensorless Integrated Single-Switch Isolated Buck-Flyback AC-DC PFC Converter Fed PMBLDCM Based CFD | 251 |

| | | |
|---------------------|---|----------------|
| 7.7.4.1 | Steady State Performance | 251 |
| 7.7.4.2 | Dynamic Performance With Supply Voltage Fluctuations | 255 |
| 7.7.4.3 | Dynamic Performance With Speed Control | 256 |
| 7.7.4.4 | Performance Comparisons at Different Operating Speeds | 257 |
| 7.8 | Comparative Evaluation of Sensorless Integrated Single-Switch Isolated AC-DC PFC Converters Fed PMBLDCM Based CFDs | 259 |
| 7.9 | Conclusions | 260 |
| CHAPTER-VIII | DESIGN, CONTROL AND IMPLEMENTATION OF HIGH-FREQUENCY BRIDGELESS AC-DC PFC CONVERTERS FED SENSORLESS PMBLDCM BASED CEILING FAN DRIVES | 261-302 |
| 8.1 | General | 261 |
| 8.2 | Configurations, Operation, and Analysis of AC-DC Bridgeless PFC Converters Fed PMBLDCM Based CFDs | 262 |
| 8.2.1 | Non-Isolated AC-DC Bridgeless SI-SEPIC PFC Converter Fed Sensorless PMBLDCM Based CFD | 262 |
| 8.2.2 | Non-Isolated AC-DC Bridgeless Coupled-Inductor Based SI-Cuk PFC Converter Fed Sensorless PMBLDCM Based CFD | 267 |
| 8.2.3 | Isolated AC-DC Bridgeless SEPIC PFC Converter Fed Sensorless PMBLDCM Based CFD | 270 |
| 8.3 | Design of AC-DC Bridgeless PFC Converters Fed Sensorless PMBLDCM Based CFDs | 274 |
| 8.3.1 | Design of Non-Isolated AC-DC Bridgeless SI-SEPIC PFC Converter Fed Sensorless PMBLDCM Based CFD | 275 |
| 8.3.2 | Design of Non-Isolated AC-DC Bridgeless Coupled-Inductor Based SI-Cuk PFC Converter Fed Sensorless PMBLDCM Based CFD | 277 |

| | | |
|---------|---|-----|
| 8.3.3 | Design of Isolated AC-DC Bridgeless SEPIC PFC Converter Fed Sensorless PMBLDCM Based CFD | 279 |
| 8.4 | Control of AC-DC Bridgeless PFC Converters Fed Sensorless PMBLDCM Based CFDs | 281 |
| 8.4.1 | Voltage Control of Non-Isolated and Isolated AC-DC Bridgeless PFC Converters | 281 |
| 8.4.2 | Back-EMF Based Sensorless Control of PMBLDCM | 283 |
| 8.5 | MATLAB Based Modeling and Simulation of AC-DC Bridgeless PFC Converters Fed Sensorless PMBLDCM Based CFDs | 284 |
| 8.5.1 | MATLAB Based Model of Non-Isolated AC-DC Bridgeless SI-SEPIC PFC Converter | 285 |
| 8.5.2 | MATLAB Based Model of Non-Isolated AC-DC Bridgeless Coupled-Inductor Based SI-Cuk PFC Converter | 286 |
| 8.5.3 | MATLAB Based Model of Isolated AC-DC Bridgeless SEPIC PFC Converter | 286 |
| 8.6 | Hardware Implementation of AC-DC Bridgeless PFC Converters Fed Sensorless PMBLDCM Based CFDs | 287 |
| 8.6.1 | Hardware Implementation of Non-Isolated AC-DC Bridgeless PFC Converters Fed Sensorless PMBLDCM Based CFD | 287 |
| 8.6.2 | Hardware Implementation of Isolated AC-DC Bridgeless SEPIC PFC Converter Fed Sensorless PMBLDCM Based CFD | 289 |
| 8.7 | Results and Discussion | 290 |
| 8.7.1 | Performance of Non-Isolated AC-DC Bridgeless PFC Converter Fed Sensorless PMBLDCM Based CFD | 291 |
| 8.7.1.1 | Steady State Performance | 291 |
| 8.7.1.2 | Dynamic Performance With Speed Control | 293 |
| 8.7.1.3 | Performance Comparisons at Different Operating Speeds | 294 |

| | | |
|-------------------|---|----------------|
| 8.7.2 | Performance of Isolated AC-DC Bridgeless SEPIC PFC Converter Fed Sensorless PMBLDCM Based CFD | 296 |
| 8.7.2.1 | Steady State Performance | 296 |
| 8.7.2.2 | Dynamic Performance With Supply Voltage Fluctuations | 298 |
| 8.7.2.3 | Dynamic Performance With Speed Control | 298 |
| 8.7.2.4 | Performance Comparisons at Different Operating Speeds | 300 |
| 8.8 | Comparative Evaluation of AC-DC Bridgeless PFC Converters Fed Sensorless PMBLDCM Based CFDs | 301 |
| 8.9 | Conclusions | 302 |
| CHAPTER-IX | MAIN CONCLUSIONS AND SUGGESTIONS FOR FURTHER WORK | 303-310 |
| 9.1 | General | 303 |
| 9.2 | Main Conclusions | 303 |
| 9.3 | Suggestions for Further Work | 309 |
| | REFERENCES | 311-327 |
| | APPENDICES | 329-334 |
| | LIST OF PUBLICATIONS | 335-337 |
| | BIO-DATA | 339-339 |

LIST OF FIGURES

- Fig.1.1 Existing flyback-PFC based CFD and its high-frequency PWM control
- Fig.1.2 (a) Toggling the AC supply switch and (b) TRIAC-Based Control of PMBLDCM-CFD
- Fig.1.3 Existing PMBLDCM based CFDs system
- Fig.1.4 Existing passive PFC for the PMBLDCM based CFD
- Fig.1.5 Existing active buck-PFC fed PMBLDCM based CFD
- Fig.1.6 Existing active flyback-PFC fed PMBLDCM based CFD
- Fig.3.1 Configurations of ceiling fan drives
- Fig.3.2 (a) PSCM and (b) its phasor representation of voltage and current
- Fig.3.3 PSCM based CFD with TRIAC control
- Fig.3.4 Outer rotor SRM based CFD with 8/6 pole configuration
- Fig.3.5 (a) Inner rotor PMSM based CFD with 12/10 pole configuration, and (b) its FOC control
- Fig.3.6 Outer rotor PMBLDCM based CFD with 18/14 pole configuration
- Fig.3.7 Screenshot of MATLAB simulation model for PSCM based CFD
- Fig.3.8 Simulation results of PSCM based CFD (a) at 115 rpm, and (b) at 350 rpm
- Fig.3.9 Screenshot of MATLAB simulation model for 8/6 pole configuration SRM based CFD
- Fig.3.10 Simulation results of SRM based CFD (a) at 115 rpm, and (b) at 350 rpm
- Fig.3.11 Screenshot of MATLAB simulation model for 12/10 pole configuration PMSM based CFD
- Fig.3.12 Simulation results of PMSM based CFD (a) at 115 rpm, and (b) at 350 rpm
- Fig.3.13 Screenshot of MATLAB simulation model for 18/14 pole configuration PMBLDCM based CFD
- Fig.3.14 Simulation results of PMBLDCM based CFD (a) at 115 rpm, and (b) at 350 rpm

- Fig.3.15 Supply side laboratory test performance of PSCM based CFD (a) 118 rpm, (b) 165 rpm (c) 217 rpm, (d) 263 rpm, (e) 326 rpm, and (f) 365 rpm.
- Fig.3.16 Harmonic contents at the supply side for PSCM based CFD (a) 118 rpm, (b) 165 rpm (c) 217 rpm, (d) 263 rpm, (e) 326 rpm, and (f) 365 rpm
- Fig.3.17 Supply side laboratory test performance of PMBLDCM based CFD (a) 118 rpm, (b) 165 rpm (c) 217 rpm, (d) 263 rpm, (e) 326 rpm, and (f) 365 rpm
- Fig.3.18 Harmonic contents at the supply side for the PMBLDCM based CFD (a) 118 rpm, (b) 165 rpm (c) 217 rpm, (d) 263 rpm, (e) 326 rpm, and (f) 365 rpm
- Fig.4.1 Circuit configurations of SI-Zeta PFC converter fed PMBLDCM based CFD
- Fig.4.2 (a)-(c) Various operating modes of a SI-Zeta PFC converter in DICM, and (d) their operating waveforms.
- Fig.4.3 (a) Equivalent linearized circuit of SI-Zeta PFC converter, (b) small-signal-model of SI-Zeta PFC converter, and (c) waveform of average output current (i_o), injected into the linear part
- Fig.4.4 Circuit configurations of PFC SIC converter fed PMBLDCM based CFD
- Fig.4.5 (a)-(c) Various operating modes of a PFC SIC converter in DICM, and (d) their operating waveforms
- Fig.4.6 (a) Linearized circuit of SIC PFC converter, (b) waveform of injected current, and (c) SSM of SIC
- Fig.4.7 (a) Coupled-inductor for sensorless SIC PFC converter, and DC-link voltage estimation using one-turn in coupled-inductor, (b) Laboratory prototype of SIC PFC converter's coupled-inductor.
- Fig.4.8 Control of SI-Zeta PFC converter fed PMBLDCM based CFD
- Fig.4.9 Closed-loop control of SI-Zeta PFC converter fed PMBLDCM based CFD
- Fig.4.10 (a) Schematic of BLDCM's sensorless control, (b) estimated virtual Hall-signal (H_a), and (c) sensorless starting.
- Fig.4.11 (a) Closed-loop control, and (b) PWM Pulses of SI-Zeta PFC converter fed PMBLDCM based CFD

- Fig.4.12 SIC PFC converter's DICM-gain and phase response without and with controller including sensor-gain
- Fig.4.13 Estimated Hall-signal ($H_{a(Estimated)}$) for the sensorless operation of PMBLDCM
- Fig.4.14 Screenshot of MATLAB simulation model of SI-Zeta PFC converter fed PMBLDCM based CFD
- Fig.4.15 Screenshot of MATLAB simulation model of coupled-inductor based sensorless SIC PFC converter for PMBLDCM based CFD
- Fig.4.16 Laboratory prototype of non-isolated SI-Zeta PFC converter fed PMBLDCM based CFD
- Fig.4.17 Laboratory prototype of sensorless coupled-inductor based non-isolated SIC PFC converter fed PMBLDCM based CFD
- Fig.4.18 (a)-(f) Steady-state performance of high-frequency non-isolated SI-Zeta PFC converter fed sensorless PMBLDCM based CFD
- Fig.4.19 (a)-(c) Harmonics distortions in the supply current under steady-state condition for the SI-Zeta PFC
- Fig.4.20 CFD's test performances with supply voltage fluctuations, i.e., (a) under voltage ($V_s = 220V-140V$), and (b) over voltage ($V_s = 220V-270V$)
- Fig.4.21 CFD's test performances with speed change; (a) 155 rpm, (b).210 rpm, (c) 268 rpm, (d) 326 rpm, (e) 378 rpm, and (f) smooth variation from 155 rpm to 378 rpm corresponding to change in $V_{DC} = 15V-48V$
- Fig.4.22 (a)-(c) Performance comparisons over a conventional PMBLDCM based CFD up to 25th harmonic order, and (d) input power at a various speeds.
- Fig.4.23 (a)-(f) Steady-state performance of high-frequency sensorless coupled-inductor based non-isolated SIC PFC converter fed PMBLDCM based CFD
- Fig.4.24 (a)-(c) Harmonics distortions in the supply current under steady-state condition for the sensorless SIC PFC converter fed PMBLDCM based CFD
- Fig.4.25 CFD's test performances with supply voltage fluctuations, i.e., (a) under voltage ($V_s = 220V-140V$), and (b) over voltage ($V_s = 220V-270V$)

- Fig.4.26 CFD's test performances with speed change; (a) 143 rpm, (b).220 rpm, (c) 260 rpm, (d) 315 rpm, (e) 350 rpm, (f) 365 rpm, and (g) smooth variation from 135 rpm to 365 rpm corresponding to change in $V_{DC} = 15V-48V$
- Fig.4.27 (a)-(c) Performance comparisons over a conventional PMBLDCM based CFD up to 25th harmonic order, and (d) power losses distribution of SIC PFC converter based CFD
- Fig.5.1 Circuit configuration of sensorless isolated AC-DC Zeta PFC converter fed PMBLDCM based CFD
- Fig.5.2 (a)-(c) Various operating modes, and (d) operating waveforms of an isolated AC-DC Zeta PFC converter in DICM
- Fig.5.3 Circuit configuration of sensorless isolated AC-DC SEPIC PFC converter fed PMBLDCM based CFD
- Fig.5.4 (a)-(c) Various operating modes, and (d) associated operating waveforms of an isolated AC-DC SEPIC PFC converter in DICM
- Fig.5.5 Circuit configuration of sensorless isolated AC-DC Cuk PFC converter fed PMBLDCM based CFD
- Fig.5.6 (a)-(c) Various operating modes, and (d) associated operating waveforms of an isolated AC-DC Cuk PFC converter in DICM.
- Fig.5.7 Estimated virtual Hall-signal (H_a) from sensed voltage (V_a)
- Fig.5.8 Screenshot of MATLAB simulation model for the sensorless Isolated AC-DC PFC converters fed PMBLDCM based CFDs
- Fig.5.9 Screenshot of MATLAB simulation model for sensorless isolated AC-DC Zeta PFC converter
- Fig.5.10 Screenshot of MATLAB simulation model for sensorless isolated AC-DC SEPIC PFC converter
- Fig.5.11 Screenshot of MATLAB simulation model for sensorless isolated AC-DC Cuk PFC converter
- Fig.5.12 Laboratory prototype of sensorless isolated AC-DC Zeta PFC converter fed PMBLDCM based CFD

- Fig.5.13 Laboratory prototype of sensorless isolated AC-DC SEPIC PFC converter fed PMBLDCM based CFD
- Fig.5.14 Laboratory prototype of sensorless isolated AC-DC Cuk PFC converter fed PMBLDCM based CFD
- Fig.5.15 (a)-(h) Steady-state performances of high-frequency sensorless isolated AC-DC Zeta PFC converter fed PMBLDCM based CFD
- Fig.5.16 Harmonics distortion in the supply current under steady-state conditions for the sensorless isolated AC-DC Zeta PFC converter fed PMBLDCM based CFD
- Fig.5.17 CFD's test performances with supply voltage fluctuations, i.e., (a) under voltage ($V_s = 220\text{V}-140\text{V}$), and (b) over voltage ($V_s = 220\text{V}-270\text{V}$)
- Fig.5.18 CFD's test performances with speed change; (a) 169 rpm, (b) 220 rpm, (c).268 rpm, (d) 320 rpm, (e) 365 rpm, (f) 405 rpm, (g) 446 rpm, (h) 465 rpm, and (i) smooth variation from 169 rpm to 465 rpm corresponding to change in $V_{DC} = 15\text{V}-48\text{V}$
- Fig.5.19 (a)-(d) Performance comparisons of an isolated Zeta PFC converter based CFD over the existing PMBLDCM based CFD
- Fig.5.20 (a)-(e) Steady-state performance of an isolated AC-DC SEPIC PFC converter based CFD
- Fig.5.21 (a)-(c) Harmonics distortions in the supply current under steady-state condition for an isolated SEPIC PFC converter based CFD
- Fig.5.22 CFD's test performances with supply voltage fluctuations, i.e., (a) under voltage ($V_s = 220\text{V}-100\text{V}$), and (b) over voltage ($V_s = 220\text{V}-270\text{V}$)
- Fig.5.23 CFD's test performances with speed change from 143 rpm to 365 rpm corresponding to change in $V_{DC} = 15\text{V}-48\text{V}$
- Fig.5.24 (a)-(f) Steady-state performance of an isolated Cuk PFC converter based CFD
- Fig.5.25 (a)-(c) Harmonics distortions in the supply current under steady-state conditions for an isolated Cuk PFC converter based CFD
- Fig.5.26 CFD's test performances with supply voltage fluctuations, i.e., (a) under voltage ($V_s = 220\text{V}-140\text{V}$), and (b) over voltage ($V_s = 220\text{V}-270\text{V}$)

- Fig.5.27 CFD's test performances with speed change from 143 rpm to 365 rpm corresponding to change in $V_{DC} = 15V-48V$
- Fig.6.1 Circuit configurations of sensorless integrated switched-inductor Buck-Flyback AC-DC PFC converter fed PMBLDCM based CFD
- Fig.6.2 (a)-(d) Various operating modes of a SI-buck-flyback PFC converter in DICM
- Fig.6.3 DICM operating waveforms of a SI-buck-flyback PFC converter
- Fig.6.4 Equivalent linearized circuit of SI-buck-flyback PFC converter
- Fig.6.5 (a) Waveform of average output current (i_o), (b) operating waveforms of diodes, and (c) small-signal model of SI-Buck-flyback PFC converter
- Fig.6.6 Circuit configurations of sensorless SEPIC-SC AC-DC PFC converter fed PMBLDCM based CFD
- Fig.6.7 (a)-(c) Different operating modes of SEPIC-SC PFC converter in DICM, and (d) their operating waveforms
- Fig.6.8 (a) Linearized circuit of a SEPIC-SC PFC converter, and (b) SSM
- Fig.6.9 (a) Closed-loop control, & (b) frequency response of SEPIC-SC PFC converter fed PMBLDCM based CFD
- Fig.6.10 (a) Block diagram of PMBLDCM sensorless control, and (b) the estimated virtual Hall-signal (H_a)
- Fig.6.11 Frequency response of SEPIC-SC PFC converter for without controller and with controller
- Fig.6.12 Laboratory prototype of sensorless integrated non-isolated single-switch SI-buck-flyback PFC converter fed PMBLDCM based CFD
- Fig.6.13 Laboratory prototype of sensorless integrated non-isolated single-switch SEPIC-SC PFC converter fed PMBLDCM based CFD.
- Fig.6.14 (a)-(f) Steady-state performance of sensorless high-frequency integrated non-isolated SI-buck-flyback PFC converter fed PMBLDCM based CFD
- Fig.6.15 (a)-(c) Harmonics distortions in the supply current under steady-state conditions for the SI-buck-flyback PFC converter fed PMBLDCM based CFD

- Fig.6.16 CFD's test performances with supply voltage fluctuations, i.e., (a) under voltage ($V_s = 220\text{V}-110\text{V}$), and (b) over voltage ($V_s = 220\text{V}-270\text{V}$)
- Fig.6.17 CFD's test performances with speed change; (a) 143 rpm, (b).260 rpm, (c) 320 rpm, (d) 350 rpm, (e) 365 rpm, and (f) smooth variation from 138 rpm to 365 rpm corresponding to change in $V_{DC} = 15\text{V}-48\text{V}$
- Fig.6.18 Performance comparisons of (a), (c) SI-buck-flyback PFC converter based CFD over the (b) existing PMBLDCM based CFD up to 25th harmonic order, and (d) Power losses distribution in presented CFD at 365 rpm
- Fig.6.19 (a)-(f) Steady-state performance of sensorless high-frequency integrated non-isolated SEPIC-SC PFC converter fed PMBLDCM based CFD
- Fig.6.20 (a)-(c) Harmonics distortions in the supply current under steady-state conditions for the sensorless SEPIC-SC PFC converter fed PMBLDCM based CFD
- Fig.6.21 CFD's test performances with supply voltage fluctuations, i.e., (a) under voltage ($V_s = 220\text{V}-90\text{V}$), and (b) over voltage ($V_s = 220\text{V}-270\text{V}$)
- Fig.6.22 CFD's test performances with speed change; (a) 116 rpm, (b).167 rpm, (c) 219 rpm, (d) 265 rpm, (e) 315 rpm, (f) 350 rpm, and (g) smooth variation from 116 rpm to 350 rpm corresponding to change in $V_{DC} = 15\text{V}-60\text{V}$
- Fig.6.23 (a)-(c) Performance comparisons of (a), (c) SEPIC-SC based CFD over the (b) existing PMBLDCM based CFD up to 25th harmonic order, and (d) power losses distribution in presented CFD at 350 rpm
- Fig.7.1 Circuit configurations of sensorless integrated single-switch Boost-Flyback AC-DC PFC converter fed PMBLDCM based CFD
- Fig.7.2 (a)-(d) Various operating modes of a single-switch boost-flyback PFC converter in DICM
- Fig.7.3 DICM operating waveforms of a single-switch boost-flyback PFC converter
- Fig.7.4 (a) Equivalent linearized circuit, and (b) Small-signal model of S⁴BF-PFC converter
- Fig.7.5 Circuit configurations of sensorless integrated single-switch isolated boost-Luo AC-DC PFC converter fed PMBLDCM based CFD

- Fig.7.6 (a)-(d) Different operating modes of integrated isolated boost-Luo PFC converter in DICM
- Fig.7.7 Operating waveforms of integrated isolated boost-Luo PFC converter in DICM
- Fig.7.8 Circuit configurations of (a) sensorless solar CFD, and sensorless integrated single-switch isolated (b) boost-flyback PFC converter, (c) boost-forward PFC converter, and (d) derived SEPIC-Forward AC-DC PFC converter fed PMBLDCM based CFD
- Fig.7.9 (a)-(e) Various operating modes of a single-switch SEPIC-forward AC-DC PFC converter in DICM, and (f) DICM operating waveforms of a single-switch SEPIC-forward PFC converter
- Fig.7.10 Circuit configurations of sensorless integrated single-switch isolated buck-flyback AC-DC PFC converter fed PMBLDCM based CFD
- Fig.7.11 (a)-(d) Different operating modes of integrated isolated buck-flyback PFC converter in DICM
- Fig.7.12 Operating waveforms of integrated isolated buck-flyback PFC converter in DICM
- Fig.7.13 (a) Output current waveform, (b) equivalent linearized circuit of IIBF-PFC converter, and (c) SSM of IIBF-PFC converter
- Fig.7.14 (a) Closed-loop control block diagram, and (b) high-frequency PWM pulses of AC-DC PFC converters
- Fig.7.15 Frequency response of control to output transfer function (G_{vd}) without and with controller for boost-flyback PFC converter
- Fig.7.16 Frequency response of control to output transfer function for different DC-link voltages (24V, 48V, 72V, and 110V)
- Fig.7.17 An estimated virtual Hall-signal (H_a) from sensed voltage
- Fig.7.18 Screenshot of MATLAB simulation model of sensorless integrated single-switch isolated AC-DC PFC converter fed PMBLDCM based CFDs
- Fig.7.19 Screenshot of MATLAB simulation model of single-switch isolated boost-flyback PFC converter

- Fig.7.20 Screenshot of MATLAB simulation model of single-switch isolated boost-Luo PFC converter
- Fig.7.21 Screenshot of MATLAB simulation model of single-switch isolated SEPIC-forward PFC converter
- Fig.7.22 Screenshot of MATLAB simulation model of single-switch isolated buck-flyback PFC converter
- Fig.7.23 Laboratory prototype of sensorless integrated single-switch isolated boost-flyback PFC converter fed PMBLDCM based CFD
- Fig.7.24 Laboratory prototype of sensorless integrated single-switch isolated boost-Luo PFC converter fed PMBLDCM based CFD
- Fig.7.25 Laboratory prototype of sensorless integrated single-switch isolated SEPIC-forward PFC converter fed PMBLDCM based CFD
- Fig.7.26 Laboratory prototype of sensorless integrated single-switch isolated buck-flyback PFC converter fed PMBLDCM based CFD
- Fig.7.27 (a)-(f) Steady-state performance of sensorless high-frequency integrated single-switch isolated boost-flyback PFC converter fed PMBLDCM based CFD
- Fig.7.28 (a)-(c) Harmonics distortions in the supply current under steady conditions for the boost-flyback PFC converter fed PMBLDCM based CFD.
- Fig.7.29 CFD's test performances with supply voltage fluctuations, i.e., (a) under voltage ($V_s = 220V-140V$), and (b) over voltage ($V_s = 220V-270V$)
- Fig.7.30 CFD's test performances with speed change; (a) 155 rpm, (b) 210 rpm, (c).268 rpm, (d) 326 rpm, (e) 378 rpm, and (f) smooth variation from 133 rpm to 378 rpm corresponding to change in $V_{DC} = 15V-48V$
- Fig.7.31 CFD's performances with DC-link voltage change corresponding to change in speed; (a)-(b) 100 rpm-378 rpm
- Fig.7.32 Performance comparisons of (a)-(c) boost-flyback PFC converter based CFD over an existing PMBLDCM based CFD, (d) Power losses distribution in the presented boost-flyback based CFD at 378 rpm, and (e) harmonics content comparisons in

the supply current (i_s) of (f) presented and (g) conventional CF system at rated speed

- Fig.7.33 (a)-(h) Steady-state performance of integrated single-switch isolated boost-Luo PFC converter fed PMBLDCM based CFD
- Fig.7.34 (a)-(c) Harmonics distortions in the supply current under steady-state conditions for an isolated boost-Luo PFC converter fed PMBLDCM based CFD
- Fig.7.35 CFD's test performances with supply voltage fluctuations, i.e., (a) under voltage ($V_s = 220V-140V$), and (b) over voltage ($V_s = 220V-270V$)
- Fig.7.36 CFD's test performances with speed change; (a) 163 rpm, (b).218 rpm, (c) 266 rpm, (d) 320 rpm, (e) 365 rpm, (f) 404 rpm, (g) 447 rpm, (h) 465 rpm and (i) smooth variation from 163 rpm to 465 rpm corresponding to change in $V_{DC} = 15V-48V$
- Fig.7.37 (a)-(d) Performance comparisons of integrated isolated boost-Luo based CFD over the existing PMBLDCM based CFD
- Fig.7.38 (a)-(g) Performance of presented 48V PMBLDCM solar CFD at the operating speed of 115 RPM, 157 RPM, 210 RPM, 260 RPM, 307 RPM, 357 RPM, and 387 RPM
- Fig. 7.39 (a)-(g) Performance of an existing 48V PMBLDCM solar CFD at the operating speed of 115 RPM, 157 RPM, 210 RPM, 260 RPM, 307 RPM, 357 RPM, and 387 RPM
- Fig. 7.40 (a)-(g) Steady-state performance of sensorless high-frequency integrated single-switch isolated SEPIC-forward PFC converter fed PMBLDCM based CFD
- Fig. 7.41 CFD's test performances with speed change; (a) 116 rpm, (b) 167 rpm, (c).219 rpm, (d) 265 rpm, (e) 315 rpm, (f) 350 rpm, and (g) 385 rpm
- Fig. 7.42 (a)-(d) Steady-state simulation performance of an integrated single-switch isolated buck-flyback PFC converter fed PMBLDCM based CFD at the DC-link voltage (V_{DC}) of 72V

- Fig. 7.43 Steady-state test performance of an integrated single-switch isolated buck-flyback PFC converter fed PMBLDCM based CFD at the DC-link voltage of (a) $V_{DC} = 24$, and (b) $V_{DC} = 110V$
- Fig. 7.44 Steady-state test performance of an integrated single-switch isolated buck-flyback PFC converter fed PMBLDCM based CFD at various DC-link voltages (a)-(b) $V_{DC}=24$, (c)-(d) 48V, (e)-(f) 72V, and (g)-(h) 110V
- Fig. 7.45 Harmonic distortions in the supply current under steady-state condition for an integrated isolated buck-flyback PFC converter fed PMBLDCM based CFD up to 25th harmonics order at the rated speed for the DC-link voltage of (a) $V_{DC}=24V$, (b) $V_{DC}=48V$, (c) $V_{DC}=72V$, and (d) $V_{DC}=110V$
- Fig. 7.46 CFD's test performances with supply voltage fluctuations, i.e., (a) under voltage ($V_s = 230V-140V$), and (b) over voltage ($V_s = 230V-285V$)
- Fig. 7.47 CFD's test performances with smooth speed variation from 118 rpm to 365 rpm corresponding to change in $V_{DC} = 15V-48V$
- Fig.8.1 Circuit configurations of non-isolated AC-DC bridgeless SI-SEPIC PFC converter fed sensorless PMBLDCM based CFD
- Fig.8.2 (a)-(c) Various operating modes of non-isolated AC-DC bridgeless SI-SEPIC PFC converter in DICM during positive half cycle of supply voltage.
- Fig.8.3 (a)-(b) DICM operating waveforms of non-isolated AC-DC bridgeless SI-SEPIC PFC converter during positive half cycle of supply voltage
- Fig.8.4 Circuit configurations of non-isolated AC-DC bridgeless coupled-inductor based SI-Cuk PFC converter fed sensorless PMBLDCM based CFD
- Fig.8.5 (a)-(c) Different operating modes of non-isolated AC-DC bridgeless coupled-inductor based SI-Cuk PFC converter in DICM during positive half cycle of supply voltage
- Fig.8.6 Circuit configurations of isolated AC-DC bridgeless SEPIC PFC converter fed sensorless PMBLDCM based CFD
- Fig.8.7 Various operating modes of isolated AC-DC bridgeless SEPIC PFC converter in DICM operation during a positive half cycle of supply voltage

- Fig.8.8 Designed coupled-inductor
- Fig.8.9 Voltage control for the bridgeless (a) non-isolated (b) isolated front-end AC-DC PFC converters
- Fig.8.10 (a)VSI fed PMBLDCM and (b) estimated virtual Hall-signal (H_a) from sensed voltage
- Fig.8.11 Screenshot of MATLAB simulation model of AC-DC bridgeless PFC converters fed sensorless PMBLDCM based CFDs
- Fig.8.12 Screenshot of MATLAB simulation model of non-isolated AC-DC bridgeless SI-SEPIC PFC converter
- Fig.8.13 Screenshot of MATLAB simulation model of non-isolated AC-DC bridgeless CIB-SIC PFC converter
- Fig.8.14 Screenshot of MATLAB simulation model of isolated AC-DC bridgeless SEPIC PFC converter
- Fig.8.15 Laboratory prototype of non-isolated AC-DC bridgeless SI-SEPIC and coupled-inductor based SI-Cuk PFC converters fed sensorless PMBLDCM based CFD
- Fig.8.16 Laboratory prototype of isolated AC-DC bridgeless SEPIC PFC converter fed sensorless PMBLDCM based CFD
- Fig.8.17 (a)-(f) Steady-state performance of high-frequency non-isolated AC-DC bridgeless PFC converters fed sensorless PMBLDCM based CFD
- Fig.8.18 (a)-(c) Harmonics distortions in the supply current under steady-state conditions for the non-isolated AC-DC bridgeless PFC converters fed sensorless PMBLDCM based CFD
- Fig.8.19 CFD's test performances with speed change; (a) 115 rpm, (b) 168 rpm, (c).218 rpm, (d) 315 rpm, (e) 354 rpm, (f) 366 rpm, and (g) smooth variation from 113 rpm to 366 rpm corresponding to change in $V_{DC} = 14V-48V$
- Fig.8.20 Performance comparisons of (a)-(b) non-isolated bridgeless AC-DC PFC converters based CFD over an existing PMBLDCM based CFD, and (c) supply current harmonics content comparison up to 25th harmonic order at 366 rpm

- Fig.8.21 (a)-(h) Steady-state performance of an isolated bridgeless SEPIC PFC converter based CFD
- Fig.8.22 (a)-(c) Harmonics distortions in the supply current under steady-state conditions for an isolated bridgeless SEPIC PFC converter based CFD
- Fig.8.23 CFD's test performances with supply voltage fluctuations, i.e., (a) under voltage ($V_s = 220V-140V$), and (b) over voltage ($V_s = 220V-270V$)
- Fig.8.24 CFD's test performances with speed change; (a) 165 rpm, (b).220 rpm, (c) 268 rpm, (d) 320 rpm, (e) 365 rpm, (f) 405 rpm, (g) 446 rpm, (h) 465 rpm and (i) smooth variation from 165 rpm to 465 rpm corresponding to change in $V_{DC} = 15V-48V$
- Fig.8.25 (a)-(d) Performance comparisons of an isolated bridgeless SEPIC PFC converter based CFD over the existing PMBLDCM based CFD

LIST OF TABLES

| | |
|-----------|---|
| Table 3.1 | Fixed and Operating Energy Cost Comparisons |
| Table 3.2 | Summarized Comparison of Lifespan, Maintenance and Common Issues for Various CFDs |
| Table 3.3 | Performance Comparisons of PSCM, SRM, PMSM, and PMBLDCM Based CFDs |
| Table 3.4 | Laboratory Test Performances of Conventional PSCM based CFD |
| Table 3.5 | Laboratory Test Performances of Conventional PMBLDCM based CFD |
| Table 4.1 | Design Parameters of SI-Zeta PFC Converter |
| Table 4.2 | Design Parameters of SIC PFC Converter |
| Table 4.3 | Switching Logics of VSI Switches ($S_1 - S_6$) |
| Table 4.4 | Parameter Specifications of SI-Zeta/SIC PFC Converters Fed PMBLDCM Based CFDs |
| Table 4.5 | Performance Comparison of SI-Zeta and SIC PFC Converter for Sensorless PMBLDCM based CFDs |
| Table 5.1 | Design Parameters of an Isolated Zeta PFC Converter |
| Table 5.2 | Design Parameters of Isolated SEPIC PFC Converter |
| Table 5.3 | Design Parameters of Isolated Cuk PFC Converter |
| Table 5.4 | VSI's Switching Logics for the Switches ($S_1 - S_6$) |
| Table 5.5 | Parameter Specifications of Sensorless Isolated AC-DC Zeta PFC Converter Fed PMBLDCM Based CFD |
| Table 5.6 | Parameter Specifications of Sensorless Isolated AC-DC SEPIC PFC Converter Fed PMBLDCM Based CFD |
| Table 5.7 | Parameter Specifications of Sensorless Isolated AC-DC Cuk PFC Converter Fed PMBLDCM Based CFD |
| Table 5.8 | Performance of PMBLDCM Based Existing CF System at a RMS Supply Voltage (V_s) = 220V |

| | |
|------------|---|
| Table 5.9 | Performance of an Isolated SEPIC PFC Converter Fed PMBLDCM Based CFD at $V_s = 220V$ |
| Table 5.10 | Performance of an Isolated Cuk PFC Converter Fed PMBLDCM Based CFD at $V_s = 220V$ |
| Table 5.11 | Performance Comparison of an Isolated AC-DC PFC Converters for PMBLDCM based CFDs |
| Table 6.1 | Design Parameters of SI-Buck-Flyback PFC Converter |
| Table 6.2 | Design Parameters of SEPIC-SC PFC Converter |
| Table 6.3 | Switching Logics of VSI Switches ($S_1 - S_6$) |
| Table 6.4 | Parameter Specifications of SI-Buck-Flyback PFC Converter Fed PMBLDCM Based CFD |
| Table 6.5 | Parameter Specifications of SEPIC-SC PFC Converter Fed PMBLDCM Based CFD |
| Table 6.6 | Performance of SI-Buck-Flyback PFC Converter Based CFD at a RMS Supply Voltage (V_s) = 220V |
| Table 6.7 | Performance of PMBLDCM Based Existing CFD at a RMS Supply Voltage (V_s) = 220V |
| Table 6.8 | Cost Comparison of Presented PMBLDCM based CFD over an Existing CFDs |
| Table 6.9 | Performance of SEPIC-SC PFC Converter Based CFD at a RMS Supply Voltage (V_s) = 220V |
| Table 6.10 | Performance of PMBLDCM Based Existing CFD at a RMS Supply Voltage (V_s) = 220V |
| Table 6.11 | Performance Comparison of SI-Buck-Flyback and SEPIC-SC PFC Converter for PMBLDCM based CFDs |
| Table 7.1 | Design Parameters of Boost-Flyback PFC Converter |
| Table 7.2 | Design Parameters of Boost-Luo PFC Converter |
| Table 7.3 | Design Parameters of SEPIC-Forward PFC Converter |
| Table 7.4 | Design Parameters of Buck-Flyback PFC Converter |

| | |
|------------|--|
| Table 7.5 | Switching Logics of VSI Switches ($S_1 - S_6$) |
| Table 7.6 | Parameter Specifications of Boost-Flyback PFC Converter Fed PMBLDCM Based CFD |
| Table 7.7 | Parameter Specifications of Boost-Luo PFC Converter Fed PMBLDCM Based CFD |
| Table 7.8 | Parameter Specifications of SEPIC-Forward PFC Converter Fed PMBLDCM Based CFD |
| Table 7.9 | Parameter Specifications of Buck-Flyback PFC Converter Fed PMBLDCM Based CFD |
| Table 7.10 | Performance of PMBLDCM Based Existing CF System at a RMS Supply Voltage (V_s) = 220V |
| Table 7.11 | Performance of PMBLDCM Based Existing CFD at a RMS Supply Voltage (V_s) = 220V |
| Table 7.12 | Performance of PMBLDCM Based Existing CFD at a RMS Supply Voltage (V_s) = 230V |
| Table 7.13 | Supply Current (i_s) Harmonics Content Comparisons |
| Table 7.14 | Performance of 48V Buck-Flyback PFC fed PMBLDCM Based CFD at the RMS Supply Voltage (V_s) = 230V |
| Table 7.15 | Performance of 48V PMBLDCM Based Existing CFD at the RMS Supply Voltage (V_s) = 230V |
| Table 7.16 | Supply Current (i_s) Harmonics Content Comparisons |
| Table 7.17 | Performance Comparison of Integrated Single-Switch Isolated PFC Converters for PMBLDCM based CFDs |
| Table 8.1 | Design Parameters of Non-Isolated Bridgeless SI-SEPIC PFC Converter |
| Table 8.2 | Design Parameters of Non-Isolated Bridgeless CIB-SIC PFC Converter |
| Table 8.3 | Design Parameters of Isolated Bridgeless SEPIC PFC Converter |
| Table 8.4 | VSI's Switching Logics for the Switches ($S_1 - S_6$) |

- Table 8.5 Parameter Specifications of Non-Isolated AC-DC Bridgeless SI-SEPIC and CIB-SIC PFC Converters Fed Sensorless PMBLDCM Based CFD
- Table 8.6 Parameter Specifications of Isolated AC-DC Bridgeless SEPIC PFC Converter Fed Sensorless PMBLDCM Based CFD
- Table 8.7 Performance of PMBLDCM Based Existing CF System at a RMS Supply Voltage (V_s) = 220V
- Table 8.8 Performance of PMBLDCM Based Existing CFD at a RMS Supply Voltage (V_s) = 220V
- Table 8.9 Performance Comparison of Bridgeless AC-DC PFC Converters for PMBLDCM based CFDs
- Table 9.1 Performance of Various AC-DC PFC Converters for PMBLDCM Based CFDs
- Table 9.2 Comparisons of Presented and Market Available CFDs
- Table 9.3 Steady-State Performance of IIBF-PFC Based CFDs at the Rated Speed with the Supply Voltage of 230V.

LIST OF ABBREVIATIONS

| | |
|----------|--|
| AC | Alternating Current |
| ACIECA | Average Current Injection Equivalent Circuit Approach |
| BL | Bridgeless |
| CF | Ceiling Fan |
| CFD | Ceiling Fan Drive |
| CCM | Continuous Conduction Mode |
| CIB-SIC | Coupled-Inductor Based Switched-Inductor Cuk |
| CrCM | Critical Conduction Mode |
| DSP | Digital Signal Processor |
| DBR | Diode Bridge Rectifier |
| DC | Direct Current |
| DICM | Discontinuous Inductor Current Mode |
| DVM | Discontinuous Voltage Mode |
| EMD | Electrical Motor Drive |
| EMI | Electromagnetic Interference |
| HFT | High-Frequency Transformer |
| HSDG | High Step Down Gain |
| IPQ | Improved Power Quality |
| IIBF-PFC | Integrated Isolated Buck-Flyback Power Factor Correction |
| IEC | International Electrotechnical Commission |
| LPF | Low Pass Filter |
| MOSFET | Metal Oxide Semiconductor Field Effect Transistor |
| PMBLDCM | Permanent Magnet Brushless Direct Current Motor |
| PMSM | Permanent Magnet Synchronous Motor |
| PSCIM | Permanent-Split Capacitor Induction Motor |

| | |
|-----------------------|--|
| PLC | Phase Lead Compensator |
| PPQ | Poor Power Quality |
| PF | Power Factor |
| PFC | Power Factor Correction |
| PWM | Pulse Width Modulation |
| SEPIC | Single Ended Primary Inductance Converter |
| SPIM | Single Phase Induction Motor |
| S ⁴ BF-PFC | Single-Stage Single-Switch Boost-Flyback Power Factor Correction |
| SPQ | Supply Power Quality |
| SC | Switched Capacitor |
| SI | Switched Inductor |
| SIC | Switched Inductor Cuk |
| SRM | Switched Reluctance Motor |
| THD | Total Harmonic Distortion |
| UPF | Unity Power Factor |
| VSI | Voltage Source Inverter |

LIST OF SYMBOLS

| | |
|-----------------------|--|
| C_a & C_b | Output Switched Capacitors |
| C_{buck} | Buck Converter Capacitor |
| C_{DC} | DC-link Capacitor |
| C_{EMI} | Electromagnetic Interference Capacitor |
| C_i | Intermediate Capacitor |
| C_{i1} & C_{i2} | Intermediate Input and Output Capacitors |
| C_o | Converter Output Capacitor |
| D | Converter Operating ON Duty |
| D_1 | Converter OFF Duty |
| D_a & D_b | High-Frequency Output Diodes of Switched Inductor Branch |
| D_{boost} | High-Frequency Boost Converter Diode |
| D_{buck} | High-Frequency Buck Converter Diode |
| D_e | High-Frequency Extra Diode |
| D_f | High-Frequency Forward Converter Diode |
| D_{fb} | High-Frequency Flyback converter diode |
| $D_{I1}=D_{I2}$ | Line Frequency Diodes |
| D_{max} & D_{min} | Maximum and Minimum Operating ON Duty |
| D_o | High-Frequency Output Diode |
| D_r | High-Frequency Reset Diode |
| D_{sig} | High-Frequency Signal Diode |
| f_{sw} | Switching Frequency (kHz) |
| i_{Lmg} | Magnetizing Current of High-Frequency Transformer |
| I_o | Average Load Current (A) |
| $i_o(t)$ | Instantaneous Load Current |
| i_s | Supply RMS Current (mA) |

| | |
|-----------------------|--|
| $i_{s(pk)}$ | Supply Peak Current (mA) |
| i_{sw} | Switch Current (mA) |
| $i_{sw(pk)}$ | Peak Switch Current |
| $(i_o)_{avg}$ | Average Output Current Before the DC-link Capacitor |
| K | Conduction Parameter |
| K_v | Constant Voltage Gain |
| L_a & L_b | Output Switched-Inductors |
| $L_{b(buck)}$ | Buck Converter Inductor |
| L_{EMI} | Electromagnetic Interference Inductor |
| L_i | Input Inductor |
| L_{mg} | Magnetizing Inductance of High-Frequency Transformer |
| L_o | Output Inductor |
| L_s | SEPIC Inductor |
| M | Gain of Converter |
| $m_k(t)$ | High-Frequency Carrier Signal |
| M_{min} & M_{max} | Minimum and Maximum Gain of Converter |
| N | Speed of CFD in RPM |
| N^* | Reference Speed of CFD in RPM |
| N_a | Auxiliary Winding Turns of High-Frequency Transformer |
| N_p | Number of Primary Turns of High-Frequency Transformer |
| $N_p/N_s=n$ | Primary to Secondary Turns Ratio of High-Frequency Transformer |
| N_r | Number of Turns in Reset Winding of High-Frequency Transformer |
| N_s | Number of Secondary Turns of High-Frequency Transformer |
| P_{in} | Input Power |
| P_{max} | Maximum Power |
| P_{out} | Output Power |
| R_{eq} | Equivalent Load Resistance |

| | |
|--------------|---|
| S_1-S_6 | Voltage Source Inverter MOSFET Switches |
| S_w | MOSFET Switch |
| T_{sw} | Switching Period |
| V_{aux} | Auxiliary Winding Voltage |
| V_{aux}^* | Reference Auxiliary Winding Voltage |
| V_c | Controlled Voltage of PI-Controller |
| V_{DC} | DC-link voltage (V) |
| V_e | Error Voltage |
| V_{GS} | Gate to Source Voltage (V) |
| V_{in} | Average Input Voltage |
| $V_p=V_{w1}$ | Primary Winding Voltage of High-Frequency Transformer |
| V_s | Supply RMS Voltage (V) |
| $V_{s(pk)}$ | Supply Peak Voltage |
| V_{sw} | Switch Voltage (V) |
| $V_{sw(pk)}$ | Peak Switch Voltage |
| V_{w2} | Secondary Winding Voltage of High-Frequency Transformer |